J Appl Electrochem (2013) 43:507–514
DOI 10.1007/s10800-013-0534-5

ORIGINAL PAPER

Influence of surface roughness on the electrochemical behavior of carbon steel

Su Kyeng Kim · In Jun Park · Dong Young Lee · Jung Gu Kim

Received: 27 September 2012 / Accepted: 7 February 2013 / Published online: 20 February 2013

Abstract The effect of the surface roughness of carbon steel on corrosion properties was investigated using electrochemical tests, and surface and Kelvin probe force microscopy (KPFM) analyses. The results of electrochemical tests show that the corrosion rate of carbon steel is increased as the surface roughness increases. It was estimated using KPFM measurement that the difference in the Volta potential between the peak and the valley increased with increasing surface roughness. As the peak has a lower potential than that of the valley, the peak acts as an anode. The surface roughness affects the Volta potential, and the Volta potential difference is inversely proportional to electron work function (EWF). The larger difference in Volta potential between the peak and valley on the rougher surface and the smaller EWF accelerated the micro-galvanic corrosion between them. The surface analyses reveal that corrosion initiated along the peak lines. The results from this study suggest that an increase of surface roughness leads to a decrease of the corrosion resistance.

Keywords Surface roughness · Volta potential · Atomic force microscopy · Kelvin probe force microscopy · Corrosion

1 Introduction

Corrosion control expenditures have enabled developed economies to sustain high levels of economic activity through the availability and reliability of their infrastructures and wealth-creating physical assets. In particular, underground steel pipe has expansive corrosion control expenditures [1]. To improve the corrosion resistance of underground steel pipe, some methods are considered such as coating [2], cathodic protection [3], and surface conditioning with mechanical treatment [4]. The surface condition strongly affects corrosion rate due to the change of electrochemical kinetics at the metal and environment interface. Thus, the relationship between the surface conditions and corrosion properties has been a matter of interest in the study of corrosion mechanisms. Among the surface condition factors, the surface roughness, which is determined by the final finishing process, has great influence on the free energy of reaction at the metal and environment interface [5, 6]. This is due to the distribution of electric current and potential at the metal surface, which results in charge transfer between the metal and the environment [7]. There are several steps of mechanical way such as shot blasting to reduce the surface roughness of underground steel pipe and the additional costs are occurred by these steps [4]. To find the most economical surface roughness condition, therefore, the relationship between surface roughness and corrosion property of underground steel pipe should be studied.

Surface roughness, in particular, has an effect on the electron work function (EWF), which is defined as the minimum energy required to remove an electron from inside a solid surface to a position just outside of it [8, 9]. In a study on the field emission process of Fe-42Ni alloy with Ba deposition, the increased surface roughness as a result of oxidation treatment caused a decrease in EWF [10]. A similar result showed that a smoother surface of indium-thin-oxide (ITO) with thin oxide film led to higher EWF [11].

S. K. Kim · I. J. Park · D. Y. Lee · J. G. Kim (✉)
School of Advanced Materials Science and Engineering, Sungkyunkwan University, 300 Chunchun-Dong, Jangan-Gu, Suwon 440-746, Republic of Korea
e-mail: kimjg@skku.ac.kr

EWF is known to be related to the electrode potential due to the reflectance of the electronic energy level on the metal surface. EWF (Φ) is equal to the Volta potential (Ψ) multiplied by the electron charge (e) [12–15]:

$$\Phi = \Psi e \quad (1)$$

When a metal comes in contact with an electrolyte, a Volta potential is established as a consequence of the electrochemical activity that occurs on the metal surface. The Volta potential was reported to vary linearly with the corrosion potential (E_{corr}) of the metal/solution interface determined using a standard reference electrode positioned in the electrolyte layer [16–19]:

$$E_{corr} = \Delta\Psi + A \quad (2)$$

where $\Delta\Psi$ is the Volta potential difference between the standard reference electrode and the metal/solution interface. A is a constant.

Metals often possess a non-uniform distribution of Volta potentials on the surface. Owing to its electrochemical nature, corrosion involves locations where the rate of the partial electrochemical reactions is the highest of those performed by surface galvanic couples. The areas exhibiting a noble potential participate in cathodic reactions, and those with a low potential, possessing a lower level of passivity, are involved in anodic dissolution [13]. Therefore, it is also possible to examine the alloy's susceptibility to microgalvanic coupling by Kelvin probe force microscopy (KPFM), which can measure the local potential distribution on the metal surface [14, 20, 21].

In this study, the effect of the surface roughness on the corrosion properties of carbon steel for underground pipe was examined by electrochemical tests and surface morphology analyses in groundwater environment. The corrosion property was analyzed with respect to the surface energy profile, which can be represented by the Volta potential as a function of surface roughness.

2 Experimental

2.1 Specimen and solution preparation

Carbon steel specimens (designated by SS400 in Korean Standards D 3503) were abraded with silicon carbide (SiC) paper of different grits (220, 600, and 1000) to create different surface roughnesses, then rinsed ultrasonically with ethanol, and dried in air. The preparation process for all specimens was completed within 10 min before the subsequent corrosion tests to obtain an identical condition of surface oxide film, which might affect the corrosion properties of the specimens. The chemical composition of SS400 steel is listed in Table 1.

Synthetic groundwater, which supplies a representative corrosive condition for steel structure exposed to soil environments at room temperature, was used as the corrosion medium [22]. Table 2 gives the chemical composition of the synthetic groundwater.

2.2 Electrochemical investigation methods

All electrochemical tests were carried out in synthetic groundwater at 25 °C. A three-electrode electrochemical system composed of a specimen, a saturated calomel electrode (SCE), and two pure graphite rods as the working, reference, and counter electrodes, respectively, was used in electrochemical experiments. The surface area of the specimens exposed to the corrosion medium was fixed at 1 cm^2 by masking the unexposed portion with well-adhered Amercoat 90 s paint. Before the electrochemical tests, the specimens were kept in solution for 1 h to obtain a stable open-circuit potential (OCP).

To verify the corrosion behavior of the steel as a function of the surface roughness, potentiodynamic polarization tests were conducted using an EG&G Model 273A potentiostat. After the specimen reached stable OCP, the potential was swept at a rate of 0.166 mV s^{-1} from a bottom potential of −250 mV_{OCP} to a top potential of 0 mV_{SCE}. Electrochemical impedance spectroscopy (EIS) measurements were carried out using a multi-potentiostat/galvanostat VMP2 at OCP with sinusoidal amplitude of 10 mV in the frequency range from 100 kHz to 0.01 Hz. The impedance data were interpreted based on an equivalent circuit using a suitable fitting procedure with ZsimpWin software. To ensure reproducibility in

Table 2 Chemical composition of synthetic groundwater (pH = 6.76)

Compound	Content (mg L^{-1})
$CaCl_2$	133.20
$MgSO_4 \cdot 7H_2O$	59.00
$NaHCO_3$	208.00
H_2SO_4	48.00
HNO_3	21.77

Table 1 Chemical composition of SS 400

Elements	C	Si	Mn	P	S	Fe
Composition (wt %)	≤0.30	–	≤0.05	≤0.05	≤1.60	Bal.

electrochemical tests, at least three measurements were taken for each specimen.

2.3 Surface analysis

The surface features were examined using atomic force microscopy (AFM) to measure the precise surface roughness of the abraded specimen with 220, 600, and 1000 grit SiC paper. In addition, the Volta potential of each abraded specimen was determined using Kelvin probe force microscopy (KPFM), which has been applied to examine the relevant electrochemical behavior of metals. The probe was made of Al–Au alloy. The vibration amplitude was 0.982 V, and the vibration frequency was set to 26 kHz. The KPFM scanning area was 100 μm^2 and the scan speed was 0.30 Hz.

The surface morphology and corrosion features of the corroded samples after 40 min of immersion in synthetic groundwater were examined using scanning electron microscopy (SEM) and an optical surface profiler.

3 Results and discussion

From the AFM analyses for specimens abraded with 220, 600, and 1000 grit SiC paper, the average surface roughness (R_a) was revealed to be 108.0, 39.3, and 16.7 nm, respectively. This indicates that an increase in SiC paper grade decreases the R_a. However, there was an insignificant difference between the actual surface areas of three specimens, which were 1.05, 1.004, and 1.001 cm^2 for R_a of 108.0, 39.3, and 16.7 nm, respectively.

Figure 1 shows the polarization curves of carbon steel as a function of the surface roughness in a synthetic groundwater solution. All steels demonstrated active corrosion behavior, such that the current density increased continuously with increasing potential. Table 3 lists the parameters obtained from Tafel extrapolation in the potentiodynamic polarization curves. The corrosion current density of the carbon steel increased with increasing surface roughness.

Figure 2 presents the Nyquist plots obtained from EIS measurements after immersion for 1 h. The high frequency region of the spectra is used to detect local surface defects, whereas the medium and low frequency spectra detect the processes within the rust and at the metal/rust interface, respectively [23]. Figure 3 shows the equivalent electrical circuit used to fit the results of the EIS tests [24], where R_s, CPE, R_{rust}, and R_{ct} represent the solution resistance, constant phase element, rust layer resistance, and charge transfer resistance, respectively. CPE was substituted for the capacitive element to give a more accurate fit [25]. CPE is used instead of a capacitor to compensate for the inhomogeneity in the system frequency. The impedance of a CPE is described by the following expression:

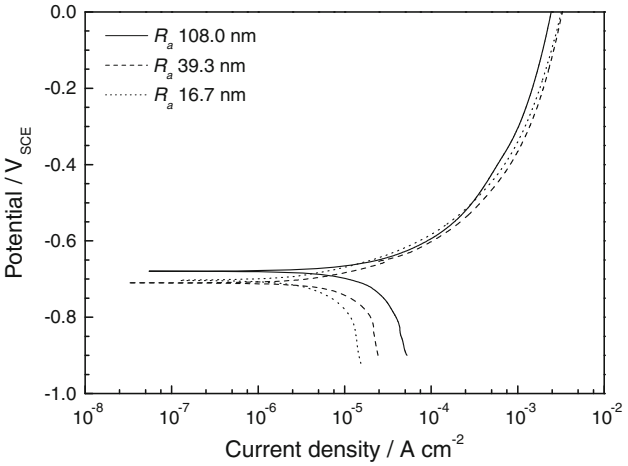

Fig. 1 Potentiodynamic polarization curves of carbon steels for different surface roughness in synthetic groundwater at 25 °C

Table 3 Results of potentiodynamic polarization tests according to the average surface roughness in a synthetic groundwater solution at room temperature

R_a (nm)	E_{corr} (mV_{SCE})	i_{corr} ($\times 10^{-6}$ A cm^{-2})	β_a (V $decade^{-1}$)	β_c (V $decade^{-1}$)
107.0	−665	10.68	0.167	0.490
39.3	−681	6.02	0.125	0.419
16.7	−680	5.96	0.130	0.507

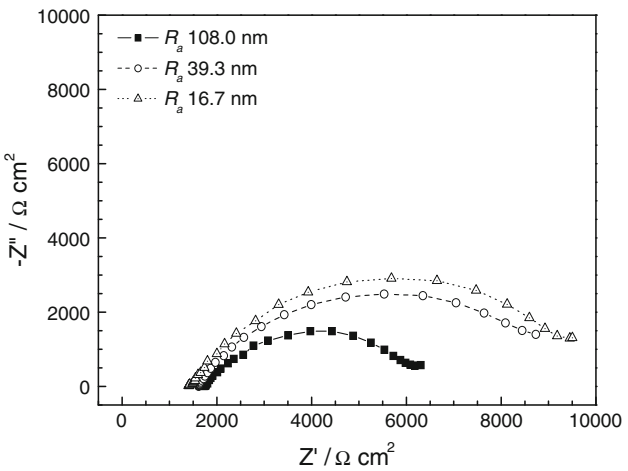

Fig. 2 Nyquist plot of impedance spectra for carbon steel as a function of average roughness

$$Z_{CPE} = A^{-1}\,(i\omega)^{-n} \tag{3}$$

where A is a proportionality coefficient (with units Ω^{-1} s^n cm^{-2}), ω is the sine wave modulation angular frequency (rad s^{-1}), $i^2 = -1$ defines the imaginary number i, and n is an empirical exponent ($0 \leq n \leq 1$) which measures the deviation from the ideal capacitive behavior [26, 27].

The ZSimpWin program of the equivalent circuit defined in Fig. 3 was used to fit the EIS data to determine the optimized values for the resistance parameters, which are presented in Table 4. The R_{rust} decreased steadily, while the R_{ct} increased strongly with decreasing surface roughness. The polarization resistance (R_p), which is the summation of R_{rust} and R_{ct}, increased with decreasing surface roughness. This is important because a high polarization resistance value indicates good corrosion resistance. From EIS results, it is suggested that the corrosion resistance of carbon steel increases with decreasing surface roughness.

From the measured Nyquist plots, depressed angles were calculated by the permutation technique suggested by Roberge [28]. By this technique, the angle between the real axis (X axis) and the depressed center of an arc projected by permuting three data points in the Nyquist plot were calculated. The depression angle is closely related to the microscopic transformation of the surface profile and can thus be a measurement of surface roughness [29]. In this study, the calculated depression angles of the Nyquist plot were 29.9, 25.0, and 14.4° for the specimens with R_a of 108.0, 39.3, and 16.7 nm, respectively. The decreasing depression can be attributed to the decreasing roughness of the surface [30, 31]. The roughness develops as a result of anodic oxidation of iron, so the depression angle acts as a measurement of the corrosion damage occurring during the exposure.

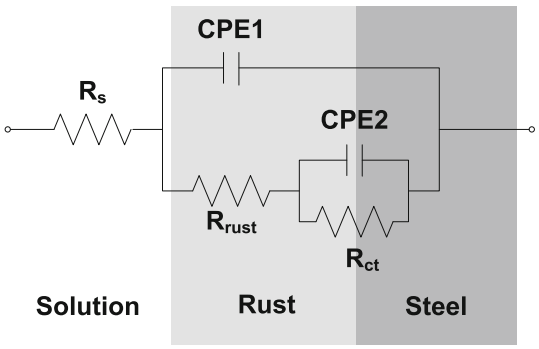

Fig. 3 Equivalent circuit for carbon steel in synthetic groundwater at 25 °C

The corrosion rate was determined using the Tafel extrapolation method based on Faraday's law [32, 33]:

$$\text{Corrosion rate (mm/year)} = \frac{3.16 \times 10^8 \times i_{corr} \times M}{z \times F \times \rho} \quad (4)$$

where i_{corr} is the corrosion current density (A cm^{-2}), M is the molar mass of the metal (g mol^{-1}), z is the number of electrons transferred per metal atom, F is Faraday's constant, and ρ is the density of the metal (g cm^{-3}). The corrosion rate decreased with decreasing R_a, as shown in Fig. 4. The corrosion rates calculated from Tafel extrapolation and EIS measurements correlated with each other. This suggests that the corrosion resistance of carbon steel can be improved by controlling the surface finish. The value of corrosion rate also shows the saturation trend below the R_a of 39.3 nm. This indicates that the critical roughness value exists to minimize corrosion rate of underground steel pipe.

Figure 5 shows a top view image of the results of the surface topography and Volta potential of the abraded specimen with different average roughness using KPFM. The brighter region indicates higher surface height and Volta potential. The Volta potential measured by KPFM

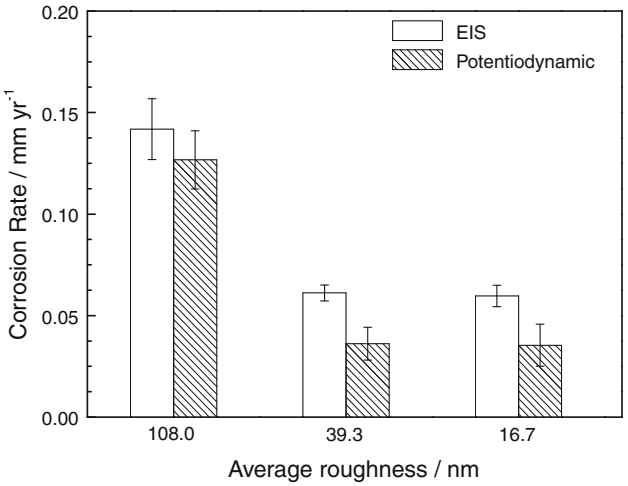

Fig. 4 Changes in corrosion rate as a function of average roughness

Table 4 Impedance parameters of carbon steel according to the average surface roughness in the synthetic groundwater at room temperature

R_a (nm)	R_s (Ω cm^2)	CPE1		R_{rust} (Ω cm^2)	CPE2		R_{ct} (Ω cm^2)
		C_{rust} (F cm^{-2})	n (0–1)		C_{dl} (F cm^{-2})	n (0–1)	
107.0	1742.8	9.0×10^{-5}	1	3019.4	5.6×10^{-5}	0.7108	1667.8
39.3	1620.1	2.1×10^{-5}	0.9276	384.4	6.6×10^{-5}	0.6449	7743.8
16.7	1432.2	1.5×10^{-5}	0.9638	266.6	8.6×10^{-5}	0.7109	8692.4

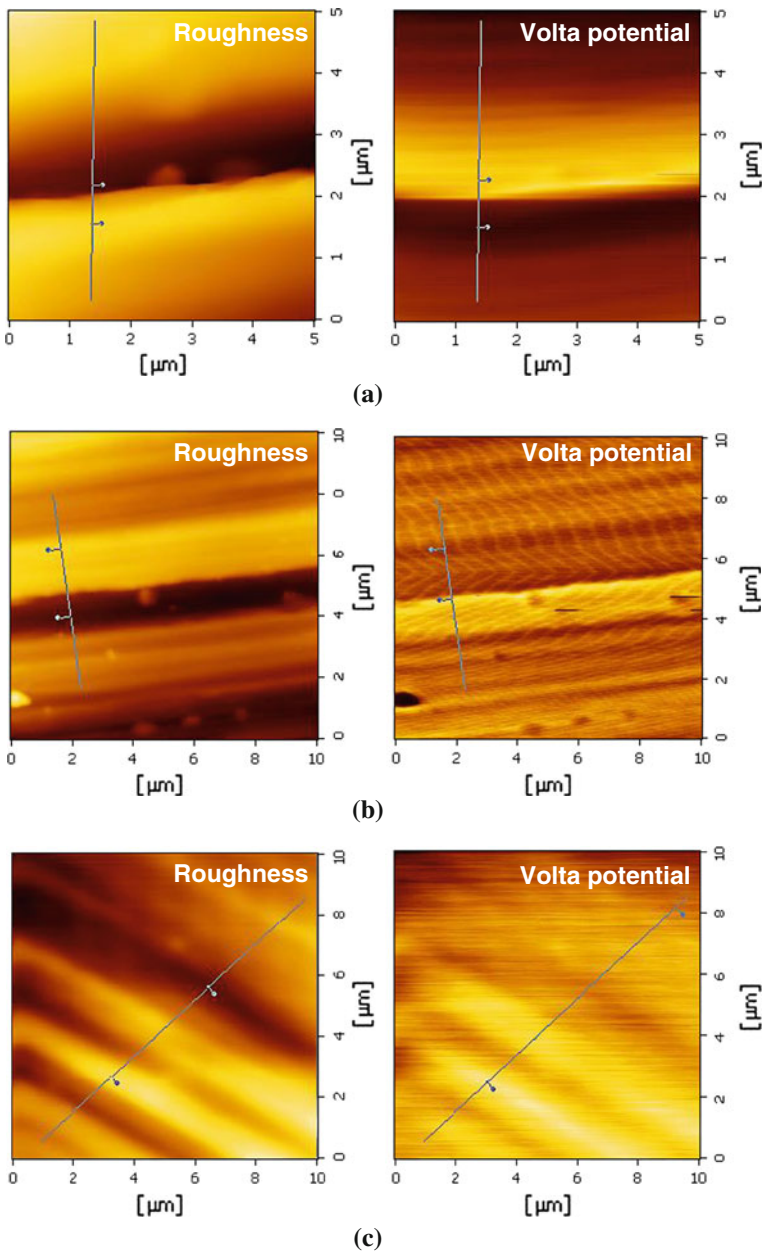

Fig. 5 Topography and Volta potential mapping image measured by KPFM with different average roughness; **a** R_a 108.0 nm, **b** R_a 39.3 nm, and **c** R_a 16.7 nm

indicates the potential difference between the probe tip and the metal surface. Thus, the Volta potential is not the absolute value, but the local profile of Volta potential on the metal surface is absolute. Figure 6a–c show the profile of surface topography and Volta potential along the inset line shown in Fig. 5. A reversed pattern between the cross-sectional topography and Volta potential was observed. The Volta potential of the valley was higher than that of the peak.

In the crystal lattice of metal, electrons are attracted by the nearest nuclei and remain in their equilibrium positions. Higher surface roughness leads to non-uniform Volta potential, which results from a distortion of the ordered surface structure. In a valley, the electrons are more confined by the surrounding nuclei. This leads to a higher potential. On the other hand, the electrons can escape easily at a peak, leading to a lower potential [11, 34]. Therefore, a difference in Volta potential between the peak and the valley was obtained, suggesting that a micro-galvanic cell can be activated between the two regions. The peak is referred to as an anode due to the lower Volta potential, whereas the less anodic property is attributed to the valley with a higher Volta potential. Therefore, the corrosion at a peak should be accelerated, whereas corrosion at a valley would be delayed. Figure 6d shows that the Volta potential difference between the peak and the valley increases with

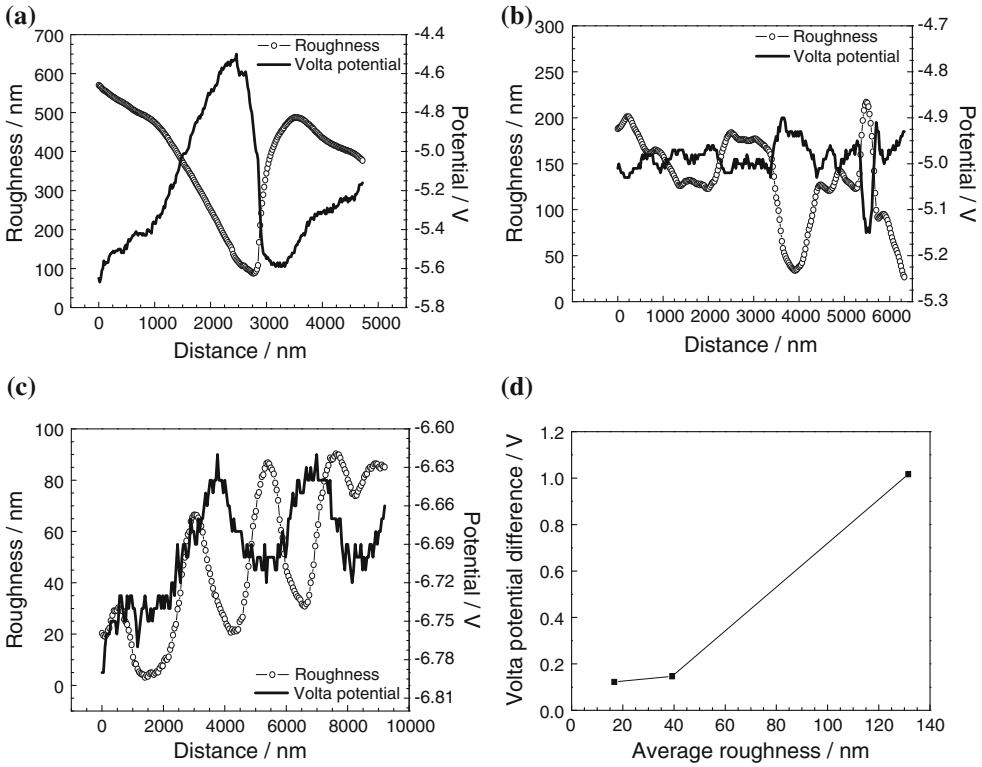

Fig. 6 Cross-sectional line diagram of roughness and Volta potential for different average roughness; **a** R_a 108.0 nm, **b** R_a 39.3 nm, **c** R_a 16.7 nm, and **d** difference of Volta potential between peak and valley with respective average roughness

increasing surface roughness, suggesting higher driving force in micro-galvanic corrosion.

In order to verify the micro-galvanic corrosion between the peak and the valley, the corroded morphology of carbon steel with R_a of 108.0 nm was observed by SEM and three-dimensional morphology analysis after immersion in synthetic groundwater for 40 min. The final corroded morphology of carbon steel after immersion test was revealed to possess a uniform corrosion aspect. It has been reported that the corrosion of carbon steel was initiated in a localized manner at the critical sites in the early stage, changing to uniform corrosion by the expansion of the localized corrosion sites [35, 36]. In this study, localized corrosion sites were observed along the abraded lines on the surface of carbon steel in the early stage of corrosion, as shown in Fig. 7a. In order to verify whether the localized corrosion sites exist along peaks or valleys, three-dimensional morphology analysis was performed. Figure 7b shows the three-dimensional image of the inset region A in Fig. 7a. It is evident that the abraded lines where the localized corrosion initiates are the peaks. These results coincide with the result that the peak acts as an anode due to the lower potential than that of valley in Fig. 6.

Considering the relationship between the result of KPFM and electrochemical tests as a function of surface roughness, R_{ct} values are obtained from EIS measurements, which are decreased (Table 4), and the Volta potential difference, which is increased (Fig. 6d) with increasing surface roughness. Previous studies also reported such an effect of roughness on the EWF. EWF was reported to vary linearly with dipole barrier, which decreases with increasing surface roughness [37, 38]. In addition, the topmost layer relaxation and surface energies of the iron surface per atom scale vary linearly with surface roughness [39]. Consequently, an increase of surface roughness decreases EWF, facilitating the movement of electrons from the metal to the surroundings. From an electrochemical point of view, easier removal of electrons corresponds to the lower value of R_{ct}, which is the resistance caused by the metal dissolution reaction. Therefore, R_{ct} decreases with increasing surface roughness.

This study presents that a decrease of surface roughness leads to an increase of the corrosion resistance. The surface roughness affects the Volta potential, and the Volta potential difference is inversely proportional to EWF. The smaller EWF and the larger difference of Volta potential between the peak and the valley on rougher surfaces accelerated the micro-galvanic corrosion between them. Several studies reported by W. Li et al. are also support these results [40–42].

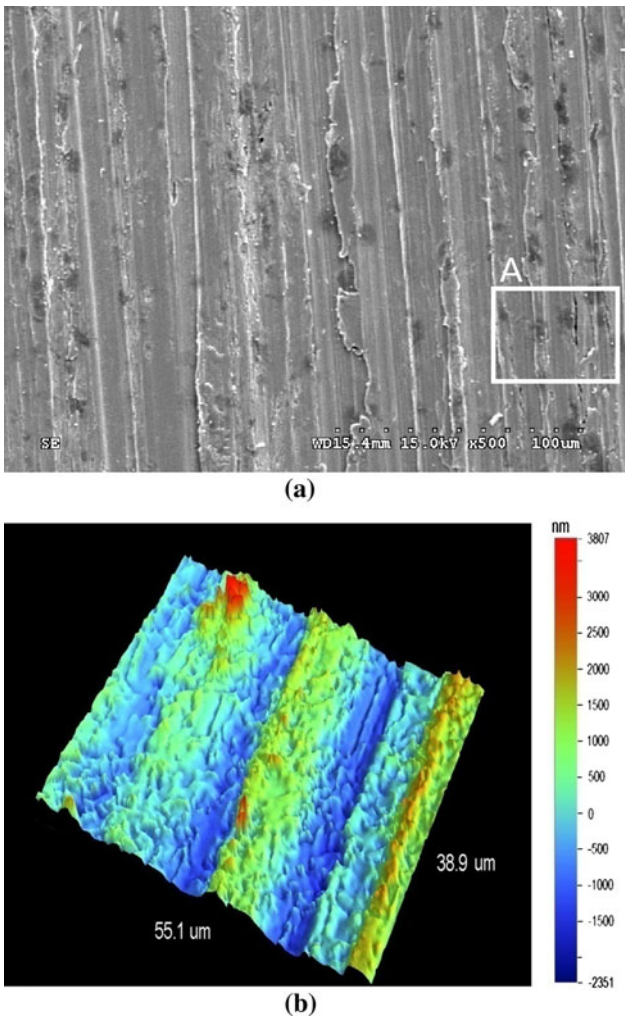

Fig. 7 Surface morphologies after 40 min of immersion; **a** SEM image and **b** optical profile image of region A in **a**

4 Conclusions

The effect of surface roughness of carbon steel on corrosion properties was investigated by electrochemical tests, and surface and KPFM analyses. In the results of the electrochemical test, the corrosion rate of carbon steel increased with increasing surface roughness. KPFM showed that the difference in Volta potential between peaks and the valleys increased with increasing surface roughness, which is referred to as micro-galvanic corrosion. The peak is referred to as an anode due to the lower Volta potential and EWF, and should act as the initiation sites of micro-galvanic corrosion, whereas the valley is referred to as a cathode due to the higher Volta potential and EWF. The larger difference in the Volta potential between the peak and the valley on a rougher surface accelerated the micro-galvanic corrosion between them. The present study also suggests that the optimal roughness value can be considered to minimize corrosion rate of underground steel pipe.

Acknowledgments This study was supported by the Korea Ministry of Knowledge Economy through the Strategic Technology Development Program.

References

1. Richardson T, Cottis B, Lindsay R, Lyon S, Scantlebury D, Scott H, Graham M (2010) Shreir's corrosion, vol 4. Elsevier, Amsterdam
2. Fontana MG (1986) Corrosion engineering. McGraw-Hill, Singapore
3. Talbot DEJ, Talbot JDR (2007) Corrosion science and technology. CRC Press, Boca Raton
4. Schulze V (2006) Modern mechanical surface treatment. Wiley-VCH, Weinheim
5. Li W, Amirfazli A (2005) A thermordynamic approach for determining the contact angle hysteresis for superhydrophobic surfaces. J Colloid Interface Sci 292:195–201. doi:10.1016/j.jcis.2005.05.062
6. Li W, Amirfazli A (2007) Microtextured superhydrophobic surfaces: a thermodynamic analysis. Adv Colloid Interface Sci 132:51–68. doi:10.1016/j.cis.2007.01.001
7. Silverman DC (2004) The rotating cylinder electrode for examining velocity-sensitive corrosion-a review. Corrosion 60:1003–1023. doi:10.5006/1.3299215
8. Ashcroft NW, Mermin ND (1976) Solid state physics. Saunders College Publishing, New York
9. Li W, Li DY (2006) Influence of surface morphology on corrosion and electronic behavior. Acta Mater 54:445–452. doi:10.1016/j.actamat.2005.09.017
10. Ozawa R, Kaykham K, Hiraishi A, Suzuki Y, Mori N, Yaguchi T, Itoh J, Yamamoto S (1999) Field emission from flat metal surfaces covered with Ba atoms. Appl Surf Sci 146:162–168. doi:10.1016/S0169-4332(99)00032-X
11. Kim JS, Cacialli F, Granström M, Friend RH, Johansson N, Salaneck WR, Daik R, Feast WJ (1999) Characterisation of the properties of surface-treated indium-tin oxide thin films. Synth Met 101:111–112. doi:10.1016/S0379-6779(98)01127-8
12. Bergveld P, Hendrikse J, Olthuis W (1998) Theory and application of the material work function for chemical sensors based on the field effect principle. Meas Sci Technol 9:1801–1808. doi:10.1088/0957-0233/9/11/003
13. Nazarov A, Thierry D (2007) Application of Volta potential mapping to determine metal surface defects. Electrochim Acta 52:7689–7696. doi:10.1016/j.electacta.2007.05.077
14. Apachitei I, Fratila-Apachitei LE, Duszczyk J (2007) Microgalvanic activity of an Mg-Al-Ca-based alloy studied by scanning Kelvin probe force microscopy. Scr Mater 57:1012–1015. doi:10.1016/j.scriptamat.2007.08.002
15. Cheran LE, Johnstone S, Sadeghi S, Thompson M (2007) Work-function measurement by high-resolution scanning Kelvin nanoprobe. Meas Sci Technol 18:567–578. doi:10.1088/0957-0233/18/3/005
16. Schmutz P, Frankel GS (1998) Corrosion study of AA2024-T3 by scanning Kelvin probe force microscopy and in situ atomic force microscopy scratching. J Electrochem Soc 145:2295–2306. doi:10.1149/1.1838634
17. Bockris JO'M, Reddy AKN (1998) Modern electrochemistry. Plenum Press, New York
18. Juzeliūnas E, Sudavičius A, Jüttner K, Fürbeth W (2003) Study of initial stages of Al-Mg alloy corrosion in water, chloride and Cu(II) environment by a scanning Kelvin probe and XPS. Electrochem Commun 5:154–158. doi:10.1016/S1388-2481(03)00015-8

19. Williams G, Holness RJ, Worsley DA, McMurray HN (2004) Inhibition of corrosion-driven organic coating delamination on zinc by polyaniline. Electrochem Commun 6:549–555. doi:10.1016/j.elecom.2004.04.004
20. Dubuisson E, Lavie P, Dalard F, Caire JP, Szunerits S (2006) Study of the atmospheric corrosion of galvanised steel in a micrometric electrolytic droplet. Electrochem Commun 8:911–915. doi:10.1016/j.elecom.2006.03.024
21. Schütze M, Cahn RW, Haasen P, Kramer EJ (2000) Corrosion and environmental degradation. Wiley-VCH, Weinheim
22. Kim JG, Kim YW, Kang MC (2002) Corrosion characteristics of rigid polyurethane thermally insulated pipeline with insulation defects. Corrosion 58:175–181. doi:10.5006/1.3277318
23. Nam ND, Kim JG (2010) Effect of niobium on the corrosion behaviour of low alloy steel in sulfuric acid solution. Corros Sci 52:3377–3384. doi:10.1016j.corsci.2010.06.010
24. Moretti G, Guidi F, Grion G (2004) Tryptamine as a green iron corrosion inhibitor in 0.5 M deaerated sulphuric acid. Corros Sci 46:387–403. doi:10.1016/S0010-938X(03)00150-1
25. Cottis R, Turgoose S (1999) Electrochemical impedance and noise. NACE International, Houston
26. López DA, Simison SN, de Sánchez SR (2003) The influence of steel microstructure on CO_2 corrosion. EIS studies on the inhibition efficiency of benzimidazole. Electrochim Acta 48:845–854. doi:10.1016/S0013-4686(02)00776-4
27. Bentiss F, Lebrini M, Vezin H, Traisnel M, Lagrené M (2009) Enhanced corrosion resistance of carbon steel in normal sulfuric acid medium by some macrocyclic polyether compounds containing a 1,3,4-thiadiazole moiety: AC impedance and computational studies. Corros Sci 51:2165–2173. doi:10.1016/j.corsci.2009.05.049
28. Roberge PR (2000) Handbook of corrosion engineering. McGraw-Hill, New York
29. Flis J, Pickering HW, Osseo-Asare K (1998) Interpretation of impedance data for reinforcing steel in alkaline solution containing chlorides and acetates. Electrochim Acta 43:1921–1929. doi:10.1016/S0013-4686(97)10004-4
30. Kramer M, Tomkiewicz M (1984) Porous electrodes. J Electrochem Soc 131:1283–1288. doi:10.1149/1.2115807
31. Nyikos L, Pajkossy T (1985) Fractal dimension and fractional power frequency-dependent impedance of blocking electrodes. Electrochim Acta 30:1533–1540. doi:10.1016/0013-4686(85)80016-5
32. Jonse DA (1996) Principles and prevention of corrosion. Prentice-Hall, NJ
33. Pound BG, Abdurrahman MH, Glucina MP, Wright GA, Sharp RM (1985) The corrosion of carbon steel and stainless steel in simulated geothermal media. Aust J Chem 38:1133–1140. doi:10.1071/CH9851133
34. Smoluchowski R (1941) Anisotropy of the electronic work function of metals. Phys Rev 60:661–674. doi:10.1103/PhysRev.60.661
35. Kim MJ, Jang YW, Yoo YH, Kim JJ, Kim JG (2010) Effect of specimen area on the corrosion rate of low alloy steel. J Korean Electrochem Soc 13:96–102. doi:10.5229/JKES.2010.13.2.096
36. Salvago G, Magagnin L, Bestetti M (2002) Unified approach to localized and general corrosion of stainless steels. Electrochim Acta 47:1787–1793. doi:10.1016/S0013-4686(02)00014-2
37. Saito S, Takeda K, Soumura T, Tani T, Maeda T (1994) Effects of surface roughness and patches on the work function of cobalt. Phys Status Solid A 142:K29–K32. doi:10.1002/pssa.2211420140
38. Lang ND, Kohn W (1973) Surface-dipole barriers in simple metals. Phys Rev B 8:6010–6012. doi:10.1103/PhysRevB.8.6010
39. Błoński P, Kiejna A (2007) Structural, electronic, and magnetic properties of bcc iron surfaces. Surf Sci 601:123–133. doi:10.1016/j.susc.2006.09.013
40. Li W, Li DY (2005) On the correlation between surface roughness and work function in copper. J Chem Phys 122:064708. doi:10.1063/1.1849135
41. Li W, Li DY (2005) Effect of surface geometrical configurations induced by microcracks on the electron work function. Acta Mater 53:3871–3878. doi:10-1016/j.actamat.2005.04.042
42. Li W, Cai M, Zong Z, Yu S (2006) Variation of surface morphology and electronic behavior under dynamic tensile conditions. Appl Phys Lett 88:181902. doi:10.1063/1.2193048